SPE 71508

Characterizing Disproportionate Permeability Reduction Using Synchrotron X-Ray Computed Microtomography

R. S. Seright, SPE, New Mexico Petroleum Recovery Research Center
J. Liang, SPE, Idaho National Engineering and Environmental Laboratory
W. Brent Lindquist, State University of New York at Stony Brook
John H. Dunsmuir, ExxonMobil Research & Engineering Company

This paper was prepared for presentation at the 2001 SPE Annual Technical Conference and Exhibition held in New Orleans, Louisiana, 30 September–3 October 2001.

Abstract

X-ray computed microtomography was used to investigate why gels reduce permeability to water more than that to oil in strongly water-wet Berea sandstone and in an oil-wet porous polyethylene core. Although the two porous media had very different porosities (22% versus 40%), the distributions of pore sizes and aspect ratios were similar. A Cr(III)-acetate-HPAM gel caused comparable oil and water permeability reductions in both porous media. In both cores, the gel reduced permeability to water by a factor 80 to 90 times more than that to oil. However, the distributions of water and oil saturations (versus pore size) were substantially different before, during, and after gel placement.

The disproportionate permeability reduction appeared to occur by different mechanisms in the two porous media. In Berea, gel caused disproportionate permeability reduction by trapping substantial volumes of oil that remained immobile during water flooding. With this high trapped oil saturation, water was forced to flow through narrow films, through the smallest pores, and through the gel itself. In contrast, during oil flooding, oil pathways remained relatively free from constriction by the gel.

In the polyethylene core, oil trapping did not contribute significantly to the disproportionate permeability reduction. Instead, oil films and a relatively small number of pore pathways provided conduits for the oil. For reasons yet to be understood, the small pore pathways appeared largely unavailable for water flow.

Introduction

Many polymers and gels can reduce the permeability to water more than that to oil or gas.[1-15] This property is critical to the success of water-shutoff treatments in production wells if hydrocarbon-productive zones cannot be protected during polymer or gelant placement.[2,3] However, the magnitude of the effect has been unpredictable from one application to the next. Presumably, the effect would be more predictable and controllable if we understood why the phenomenon occurs. Although many mechanisms have been considered (see Table 1), the underlying cause of the disproportionate permeability reduction remains elusive.

Previously, we used NMR imaging to observe disproportionate permeability reduction on a microscopic scale.[16] Results from these experiments revealed that the imaging technique had many limitations that prevented us from obtaining reliable pore-level images. Most importantly, the spatial resolution was on the order of hundreds of micrometers, which was too low to clearly distinguish fluid pathways on the pore level.

In this paper, we describe imaging experiments using high-resolution computed X-ray microtomography (XMT) to compare the oil and water pathways and fluid distributions before and after gel treatment. The current generation of synchrotron based XMT scanners provide the ability to obtain three-dimensional pore-level images of rock samples with a spatial resolution on the order of micrometers.[17-23] For this study, we used the ExxonMobil beamline X2-B at the National Synchrotron Light Source.[18] X2-B is a dedicated XMT imaging facility capable of producing continuous registered stacks of 2048 x 2048 x 1024 14-bit three-dimensional images of X-ray linear attenuation coefficients at energies tunable from 8 to 40 keV. The highly collimated synchrotron X-rays permit the reconstruction of a three dimensional image from two-dimensional projections taken at uniformly spaced angles between 0 and 180 degrees. X2-B converts the pattern X-rays transmitted by the specimen (projections) to a visible light image using a thin single crystal

of CsI(Na). This image was magnified by an optical microscope objective onto a 1024x1024 charge coupled device (CCD). Using Fourier methods, the set of angular projections at each row of pixels in the CCD was used to reconstruct the cross-sectional slice at that row. These slices were stacked to form the three-dimensional image. In this work, a 5x microscope objective was used to provide a pixel size of 4.1 ?m and a 4.1-mm field of view. Since part of the core was outside the imaged area, a profile extension method was used to supress edge artifacts.

Several authors used XMT to characterize the microscopic structure of porous media.[17,19,23] For a 15-darcy sandstone, Coles *et al.*[19] found a mean tortuosity of 2.7, with a range from 1.5 to 4.5. Along a 2.2-mm-long section of this core, porosity varied only a few percent around the average value (26.4%). After oil flooding, this core was water flooded to a water saturation of 25.1%. Interestingly, large variations in water saturation were observed along the 2.2-mm-long section—ranging from 12% to 39%. A three-dimensional view showed the non-wetting phase (water in this case) to exist as large ganglia (blobs of non-wetting phase that extend over multiple pores—often exhibiting a branched structure).[19]

Chatzis *et al.*[24,25] suggested that rock heterogeneity can be responsible for saturation variations within a porous medium. Non-wetting phase saturations that are lower than expected can occur when clusters of small pores are dispersed in a matrix dominated by large pores. In contrast, non-wetting phase saturations that are higher than expected can occur when clusters of large pores are dispersed in a matrix dominated by small pores.[24] However, significant saturation variations can occur even in homogeneous porous media, depending on the pore body/pore throat aspect ratio. For homogeneous 2-dimensional micromodels, Chatzis *et al.*[24] reported piston-like displacements with very little trapping of the non-wetting phase when the aspect ratio was two or less. However, for aspect ratios around 3, large non-wetting phase clusters formed as the wetting phase formed fingers while displacing the non-wetting phase. At higher aspect ratios, the non-wetting phase tended to be trapped in individual pores rather than in large clusters of pores. The pore coordination number had a minor effect on non-wetting phase residual saturations.[24]

Using XMT data, Lindquist *et al.*[23] extensively characterized pore and throat size distributions for Fontainebleau sandstones. As core porosity increased from 7.5% to 22%, they found that the average pore coordination number increased from 3.4 to 3.8, the average channel length decreased from 200 to 130 μm, the average throat area increased from 1,600 to 2,200 μm^2, and the average pore volume remained fairly constant at around 0.0004 mm^3. The average aspect ratio (effective average pore radius/effective average throat radius) was around 2.

Experimental Materials

We performed two sets of imaging experiments using strongly water-wet Berea sandstone cores and one set using a polyethylene core, which was strongly oil-wet. (The water-advancing contact angle was measured at 165 degrees for the brine/oil/polyethylene system used in this work.) The Berea cores had permeabilities of ~0.47 darcys and porosities of 22%. The polyethylene core had a permeability of 8.8 darcys and a porosity of 40%. (Consistent porosity values were determined from both image analyses and conventional mass balance measurements.) The cores were 6.5 mm in diameter and 30 mm in length, with an intermediate pressure tap 6 mm from the inlet face. Our scans focused on a segment of the core that was 6.5 mm in diameter and 3.25 mm in length. To avoid end effects, the scanned segment was located about half way between the inlet and outlet faces. The brine used during the water floods contained 1% NaCl, and 0.1% $CaCl_2$. A hexadecane mixture was used during the oil floods. To increase the image contrast between the brine and oil phases, hexadecane was doped with 10% w/w iodohexadecane in our first set of experiments in Berea and with 15% w/w bromohexadecane in the second set. For the polyethylene core, the hexadecane was doped with 15% w/w bromohexadecane. All experiments occurred at room temperature. The gelant used in these experiments contained 0.5% Alcoflood 935 HPAM (molecular weight ?5x10^6 daltons; degree of hydrolysis 5% to 10%), 0.0417% Cr(III) acetate, 1% NaCl, and 0.1% $CaCl_2$. The gelant viscosity at room temperature was 20 cp. The viscosities were 1.0 cp for brine (without polymer), 3.3 cp for the hexadecane/iodohexadecane mixture, and 3.6 cp for the hexadecane/bromohexadecane mixture.

Core Characterization

Three-dimensional scans were performed after a gelant flood and after oil and water floods both before and after gel placement. (Images were acquired at saturation endpoints.) All floods in a given set of experiments were conducted without removing the core from the sample stand so that the images could be compared directly. For each scan the image was cropped into a 2.97 mm ? 2.97 mm ? 2.1 mm rectangular block (the images were 725x725x512 voxels at 4.1 μm/voxel) to remove artifacts caused by those parts of the core that did not remain within the field of view through all 180 degrees of sample rotation. Image analyses were performed using a software package called 3DMA—a statistical analysis tool that correlates saturations with geometry. This software is capable of measuring distributions of pore size, pore-body/pore-throat aspect ratio, and coordination number of a porous rock using our three-dimensional images. The methods used to make these characterizations are described in Ref. 23. To visualize the pore structure and fluid locations, we first focused on thin cross-sections with dimensions of 1.15 mm ? 1.15 mm in the *x-y* directions (i.e., perpendicular to the flow direction). Figs. 1 and 2 compare the image cross-sections for the first Berea core when first saturated with brine and for the polyethylene core when first saturated with oil. The black areas show rock grains or polyethylene. The white areas show brine-saturated voids in the Berea and oil-saturated voids in the polyethylene. These figures highlight the irregular sizes and shapes of the voids. Although, the porosity difference is noticeable (22% for

Berea and 40% for polyethylene), the pore body and throat sizes were comparable. Electron micrographs (Figs. 3 and 4) were obtained at high magnification for Berea and polyethylene to illustrate the character of the pore walls. (These images were obtained using a Cameca SX100 electron microprobe at the New Mexico Bureau of Mines.) Due to a coating of kaolinite, a significantly greater surface roughness and angularity existed in Berea (Fig. 3) than in the polyethylene core (Fig. 4). Interestingly, thin filaments (~0.1-?m diameter) bridged many of the small pores in polyethylene (Fig. 4). Although not shown, these filaments were not seen in the larger pores.

Size distributions. The pore size distributions for two Berea cores and the polyethylene core are shown in Fig. 5. The *y*-axis plots the percent of the total number of pores that had a given pore volume (indicated on the *x*-axis). The distributions (based on pore numbers) were similar for the three cores. For pores with volumes below 0.0003 mm^3, the fraction of pores of a given size was fairly insensitive to the pore volume. Above 0.0003 mm^3, the concentration of pores decreased significantly with increased pore volume.

Pore volume distributions for the three cores are shown in Fig. 6. The *y*-axis plots the percent of the total void volume that existed in pores with a given size (indicated on the *x*-axis). Again, the distributions were quite similar, considering the material differences. The peak in the pore volume occurred at an effective pore radius (assuming spherical pores) about 50 ?m for the first Berea core, 70 ?m for the second Berea core, and 70 ?m for the polyethylene core. The average nodal pore volumes for the three cores were very similar to those found by Lindquist *et al.*[23] for Fontainebleau sandstones (~0.0004 mm^3). A comparison of Figs. 5 and 6 reveals that although many pores existed with volumes less than 0.0001 mm^3, their contribution to the total void volume was small.

Aspect Ratios. The distribution of aspect ratios (effective pore radius/effective throat radius) for the Berea and polyethylene cores are shown in Fig. 7. (The effective pore radius assumed that the pore was spherical. The effective throat radius assumed that the throat area was circular.) The *y*-axis plots the average aspect ratio in pores with a given size (indicated on the *x*-axis). Again, the distributions were surprisingly similar for the cores. The average aspect ratio was 4.0/1 for the first Berea core, 4.2 for the second Berea core, and 4.4/1 for the polyethylene core. As pore volume increased from 10^{-5} mm^3 (effective pore radius ~13 ?m) to 0.002 mm^3 (effective pore radius ~78 ?m), the average aspect ratio increased steadily from 2 to 6. Aspect ratios jumped sharply for the few largest pores. For a given pore size, a wide range of aspect ratios were noted. For all cores at a given pore size, the standard deviation (of aspect ratios) was typically 65% of the mean value.

For Berea sandstone, Fig. 8 plots the distributions of aspect ratios for each of four ranges of pore volume (PV): (1) PV>0.01 mm^3, (2) 0.001<PV<0.01 mm^3, (3) 0.0001<PV<0.001 mm^3, and (4) PV<0.0001 mm^3. The *x*-axis plots various ranges of aspect ratio, *R*, from *R*<2 up to *R*>30. The *y*-axis plots the percent of the total aspect ratios (for a given PV range) that falls within a given range of aspect ratios. The solid and open triangles in Fig. 8 show that about 35% of the smallest pores were associated with aspect ratios that were less than 2. Interestingly for all four pore-size ranges, 25-35% of the aspect ratios fell between 3 and 5, and a significant percentage of aspect ratios fell between 5 and 10. Aspect ratios above 10 were common for the larger pores but were rare for the smaller pores. In contrast, aspect ratios below 3 were very common for the smaller pores but were much less frequent for the larger pores.

The average throat area was 1,330 μm^2 for the first Berea core, 1,460 μm^2 for the second Berea core, and 1,630 μm^2 for the polyethylene core. These values were generally lower than the average throat areas reported for Fontainebleau sandstones (1,600 to 2,200 μm^2).[23]

Coordination Numbers. The distributions of pore coordination numbers are shown in Fig. 9. (The coordination number is the number of exits from a pore.) The *y*-axis plots the average coordination number in pores with a given size (indicated on the *x*-axis). The average coordination number was 3.9 for the first Berea core, 4.7 for the second Berea core, and 6.2 for the polyethylene core. For the smallest pores, the coordination number was around three for all three cores. As the pore size increased, the coordination numbers increased—with the polyethylene core experiencing a slightly more rapid increase than the Berea cores. Coordination numbers up to 70 were noted for the largest pores. For a given pore size, standard deviations were typically 20% to 40% of the mean values.

Images After the Various Floods

XMT scans were performed after each flood. Fig. 1 and Figs. 10-15 show image slices for the first Berea core for each of the flooding stages. Fig. 2 and Figs. 16-21 show image slices for the various flooding stages in the polyethylene core. In Figs. 10-21, oil is red, water is green, and the rock grains (or polyethylene) are black. To magnify the pore structure, these cross-sections are 1.15 mm x 1.15 mm. Corresponding fluid saturations and permeabilities associated with the floods are listed in Tables 2 and 3.

Berea Sandstone Image Analyses

Before Gelant Injection. In the first Berea core, the first scan viewed the core with 100% brine saturation (Fig. 10). Second, the core was flooded with ~35 core pore volumes of oil and scanned at residual water saturation (Fig. 11). Oil invaded most pores while the residual water appeared dominantly in crevices and films between oil and the rock. The residual water saturation, S_{wr}, was 24.7% (Table 2), and the endpoint relative permeability to oil (relative to the absolute permeability), k_{ro}, was 0.82 (Table 3). Third, the core was flooded with water (~70 core pore volumes) and scanned at residual oil saturation (Fig. 12). The residual oil occupied the centers of the pores while water formed a film around the

residual oil. The residual oil saturation, S_{or}, was 43.5% (i.e., 100%-56.5%, from Table 2), and the endpoint relative permeability to water, k_{rw}, was 0.16. These findings are consistent with expectations in a strongly water-wet rock.

Using the 3DMA software, detailed analyses were performed using the complete three-dimensional images (not just the two-dimensional slices shown in Figs. 10-21). The distributions of water and oil saturations were determined as a function of pore size. In Fig. 22, the solid symbols show the distribution of water saturations (S_w) at S_{wr} before gel placement. (In this figure and subsequent figures, average saturations for a given pore size are reported.) The open symbols show the distribution of water saturations at S_{or} before gel placement. (Of course, at any condition, the oil saturation is equal to 100% minus the water saturation.) As mentioned, the overall average S_{wr} was 24.7% for the first Berea core. This number was consistent with S_{wr} values measured using mass balances in this strongly water-wet Berea sandstone. As expected at S_{wr}, the water saturation generally increased with decreased pore size (solid circles in Fig. 22). A broad minimum in water saturation was noted around 0.002 mm^3, and a local maximum was observed around 0.01 mm^3. For a strongly water-wet porous medium, one might have expected the water saturation to approach 100% for the smallest pores. Instead, the water saturation in the smallest pores averaged 60%. A calculation using the Laplace equation confirmed that oil should be able to enter the smallest pores in our Berea cores. Specifically, to enter the smallest pore throats (~7 ?m), a capillary pressure around 1 psi was needed. This value was much lower than the 17 psi (pressure drop across the core) that was applied during our flooding experiments. The behavior of S_w versus pore size was confirmed during an imaging experiment in a second Berea core (solid squares in Fig. 22). This experiment included a second oil flood (following an intervening water flood). Results from this part of the experiment (solid triangles in Fig. 22) further confirmed the above behavior and indicated minimum hysteresis during cycles of water and oil flooding before gel placement. The fluid saturations and relative permeabilities from this second Berea core (Tables 2 and 3) also suggest that little hysteresis occurred during multiple flooding cycles.

As mentioned, the overall average S_{or} was 43.5% for the first Berea core. This number was significantly higher than the S_{or} values measured using mass balances in this strongly water-wet Berea sandstone (~22%). At S_{or}, the average water saturation was surprisingly insensitive to pore size (open circles in Fig. 22). The above results were confirmed during imaging studies of our second core (open squares in Fig. 22).

For a given pore size, Fig. 22 shows the average water saturation from a given experiment. Of course, since many pores were present for any given pore size, a range of saturations was found. A detailed examination of the data revealed that for a given pore size, the range or distribution of water saturations was broader at S_{or} than at S_{wr}.

During Gelant Injection. After establishing a residual oil saturation in the first Berea core, the 20-cp Cr(III)-acetate-HPAM gelant (10 core pore volumes) was injected using a pressure gradient of 17 psi/ft. After gel placement, the core was shut in for twelve hours (at 60°C) and then scanned (at room temperature). The gelation time for this formulation was 1 to 1.5 hours at 60°C.

A comparison of Figs. 12 and 13 suggests that fluid saturations changed somewhat during gelant injection. In particular, oil apparently was displaced from one of the larger pores. A detailed analysis of the three-dimensional images (Fig. 23) confirmed that fluid saturations changed during gelant injection. The open and solid circles in Fig. 23 reveal that average water saturations decreased slightly in the medium to large pores during gelant injection in Berea. Also, the overall average water saturation decreased from 56.5% to 47.7% (Table 2). On first consideration, these observations surprisingly suggest that oil was generated when gelant (containing no oil) was injected. However, the reader should recall that the imaged volume constituted only 10% of the total core volume. Conceivably, oil was displaced from upstream portions of the core during gelant injection, and this oil became trapped in the imaged volume by coincidence. Presumably, the overall oil content of the core either stayed the same or decreased slightly during gelant injection.

After Gel Placement. After gel placement, oil (~20 core pore volumes) was injected to measure the oil residual resistance factor, F_{rro}—recording a value of 15. This value means that at S_{wr}, the gel reduced the permeability to oil by a factor of 15. The core was scanned after oil injection to visualize oil pathways after gel (Fig. 14). A comparison of Figs. 11 and 14 indicates that most of the pathways open to oil flow before gel placement remained accessible to oil after the gel treatment. This result suggests that the gel occupied only a small fraction of the pore space. Tracer results from a previous experiment in a high-permeability Berea core revealed that gel with an F_{rro} value of 20 occupied less than 5% of the pore space.[1]

The solid symbols in Fig. 24 compare distributions of water saturations at S_{wr} before versus after gel placement. The two distributions were remarkably similar, confirming that most of the pathways that were open to oil flow before gel placement were also open to oil flow after gel placement. As mentioned above, this suggestion is consistent with the relatively low oil residual resistance factor (i.e., 15). Since the gel was placed and formed at high water saturation in the core, the result also suggests either (1) gel did not form in all the aqueous pore space (i.e., gelation was incomplete) or (2) oil flooding after gel placement moved, concentrated, or destroyed much of the gel that formed in the oil pathways.

Finally, brine (2.5 core pore volumes) was injected to measure the water residual resistance factor, F_{rrw}. The F_{rrw} value was 1,220—meaning that at S_{or}, the gel reduced the permeability to water by a factor of 1,220. This gel reduced the permeability to water 81 times more than that to oil (F_{rrw}/F_{rro}=81). Fig. 15 shows the core scan after brine injection. A comparison of Figs. 12 and 15 shows that water

did not have access to most of the pathways that were open to oil flow after the gel treatment.

The open symbols in Fig. 24 compare distributions of water saturations at S_{or} before versus after gel placement. For reasons yet to be explained, water saturations in the smallest pores (<0.0005 mm^3) at S_{or} after gel placement were less than those at S_{wr}. However, more importantly (because the total pore volume was dominated by the largest pores), the distribution of water saturations in the largest pores (>0.001 mm^3) after gel placement during water flooding (open triangles) was similar to that during the previous oil floods (solid symbols in Figs. 22 and 24). Therefore, the gel treatment apparently trapped substantial additional volumes of oil during water flooding (i.e., much higher S_{or} values). Perhaps, this result occurred because gel was strategically positioned in pore throats to increase aspect ratios. With the larger pores permanently occupied by oil, water was forced to flow through narrow films, through the smallest pores, and through the gel itself—explaining the large water residual resistance factor (i.e., 1,220). In contrast, oil pathways remained relatively free from constriction by the gel, so the oil residual resistance factor was much less (i.e., 15).

Polyethylene Image Analyses

Before Gelant Injection. In the polyethylene core, the first scan viewed the core with 100% oil saturation (Fig. 2). Second, the core was water flooded (~70 core pore volumes) and scanned at residual oil saturation (Fig. 16). Water invaded most pores while the residual oil appeared dominantly in small pores and films between water and the polyethylene. The oil films were less evident than the water films in Berea (compare Figs. 11 and 16); however, careful examination reveals that the oil films were present on the polyethylene. In reality, the liquid films should be much thinner than we can resolve with the XMT method. The appearance that water films on Berea sandstone were thicker than oil films on polyethylene may be caused by the greater surface roughness in Berea (compare Figs. 3 and 4). Greater surface roughness creates folds of the film and fluid accumulations in nooks and crannies. Although the actual film thickness may be only a few tens of nanometers at a given point, the film folds and small fluid accumulations are interpreted to be much wider using our imaging technique (because the resolution is limited to the micrometer scale).

Third, oil (~35 core pore volumes) was injected to drive the core to residual water saturation (Fig. 17). Residual water was noted in pores with a wide range of sizes. Also, water often appeared at the polyethylene interface—suggesting either very thin oil films or partial water wetting of the plastic.

Water (~70 core pore volumes) was again injected to establish S_{or} (Fig. 18). The similarity of Figs. 16 and 18 indicates little hysteresis during the cycle of water and oil injection. The similarity of water saturations (77.7% versus 75.0%) and relative permeabilities (0.50 versus 0.49) for the two water floods at S_{or} supports this suggestion (Tables 2 and 3). Fig. 25 provides additional support. This figure plots water saturations as a function of pore size before gelant injection. The solid circles show the distribution of water saturations at S_{wr} before gel placement. The open circles and triangles show the two distributions at S_{or}. The similarity of the two distributions at S_{or} confirms that hysteresis was not significant.

A comparison of Figs. 22 and 25 reveals significant differences in the saturation distributions for Berea versus polyethylene. Most notably, the intermediate-to-large pores exhibited a substantially greater saturation difference between S_{wr} and S_{or} for polyethylene (~15% versus ~85%) than for Berea (~30% versus ~60%). For the smallest pores in both porous media, the distributions at S_{wr} converged with those at S_{or}. However, the water saturation for this convergence occurred at a significantly lower value for polyethylene (10%-20%) than for Berea (50%-60%). For polyethylene, the average water saturation at S_{wr} was nearly independent of pore size. In contrast, in Berea, the average water saturation at S_{or} was nearly independent of pore size. For polyethylene at S_{or}, the water saturation increased significantly with increased pore size. In contrast, for Berea at S_{wr}, the water saturation decreased significantly with increased pore size. Presumably, these differences reflect the preference for water to occupy the smallest pores in water-wet Berea and not to occupy the smallest pores in the oil-wet polyethylene (i.e., because the ratio of surface area to volume increased with decreased pore size).

During Gelant Injection. In the next step, gelant (10 core pore volumes) was injected using a pressure gradient of 23 psi/ft. After gel placement, the core was shut in for 14 hours (at ~70°C) and scanned (at room temperature). A comparison of Figs. 18 and 19 indicates that oil was mobilized during gelant injection. Immediately after gel placement, most remaining oil appeared as a film attached to the polyethylene. Although a water residual resistance factor was not measured at this point, in a separate study,[13] an F_{rrw} value of 25,000 was measured for this gelant and core material immediately after gel placement. This high residual resistance factor indicated that the gel occupied virtually all of the aqueous pore space and reduced the core permeability to about 200 μD.

A detailed analysis of the three-dimensional images (Fig. 23) confirmed that fluid saturations changed during gelant injection. The open and solid triangles in Fig. 23 reveal that average water saturations increased substantially in the small-to-medium pores during gelant injection in polyethylene. Also, the overall average water saturation increased from 75.0% to 94.4% (Table 2). On the one hand, an increase in water saturation might be expected since the injected gelant was 20 times more viscous than the displaced water. However, on the other hand, the pressure gradient during gelant placement (23 psi/ft) was intentionally kept below that used during the other flooding steps (35 psi/ft) to avoid mobilization of the residual phase. Three arguments could be offered to rationalize the observed behavior. First, because polyethylene was oil wet, a continuous oil film may have existed throughout the porous medium. Thus, true irreducible oil saturation may not exist. With increased gelant or water throughput, oil in the continuous film may be able to drain slowly from the porous medium. A second explanation is that the gelant may have

changed the wettability of the porous medium to more water-wet. However, although some argue in favor of this type of mechanism,[26] it is counterintuitive and requires much more convincing support. A third possible mechanism was suggested by Wang *et al*.[27] Specifically, at a fixed capillary number, viscoelastic polymer solutions (e.g., our gelant) redistribute forces on a microscopic scale in a manner that drives residual phases to lower than expected values. These possibilities will be explored during future work.

After Gel Placement. After the shut-in period, oil (20 core pore volumes) was injected and a value of 24 was measured for the oil residual resistance factor. This value was quite similar to the corresponding value measured in Berea (i.e., 15, from Table 3). However, a comparison of the XMT scans (Figs. 14 and 20) suggests that the oil saturations and oil pathways were very different in polyethylene than in Berea. In Berea, the overall oil saturation was quite high (71%, from Table 2). In polyethylene, the oil saturation was much lower (24.3%, from Table 2). Interestingly, the oil locations in Fig. 20 were very similar to those in Figs. 16 and 18. Thus, in polyethylene, the oil locations during oil injection after gel placement were virtually the same as those during water injection before gel placement. This observation receives further support from the plots of water saturation versus pore size. In Fig. 26, the saturation distribution at S_{or} before gel placement (open circles) was virtually the same as that at S_{wr} after gel placement (solid triangles).

Finally, water (2.5 core pore volumes) was injected and a value of 2,130 was measured for F_{rrw}. This value was comparable to that for Berea (i.e., 1,220, from Table 3). Also, the ratio, F_{rrw}/F_{rro}, was 89 in polyethylene versus 81 in Berea. In spite of the similarity of F_{rrw} values, the water saturations and water pathways appear very different in polyethylene than in Berea (compare Figs. 15 and 21). In Berea, a comparison of Figs. 14 and 15 suggests that the dramatic permeability reduction for water was caused by gel trapping a high residual oil saturation. In contrast, in polyethylene (Fig. 21), the oil saturation was very low (7.6% from Table 2). Interestingly, the images shown in Figs. 19 and 21 are very similar. This observation receives further support from the plots of water saturation versus pore size. The saturation distribution at S_{or} immediately after gel placement (solid triangles in Fig. 23) was very similar to that after the final water flood after gel placement (open triangles in Fig. 26).

Presumably during gelant injection, virtually all water was displaced by the aqueous gelant. As mentioned earlier, some "residual" oil was displaced also. After gelation, an effective gel permanently occupied locations that were previously occupied by water at S_{or} before gelant injection. Thus, oil could no longer flow through those locations. The only flow paths available for oil were those through locations that were occupied by oil at S_{or} before gelant injection. This scenario explains why the distribution of saturations at S_{or} before gelant injection was the same as that at S_{wr} after gel placement (Figs. 18, 20, and 26). However, at the condition associated with S_{or}, why should oil be able to flow at all? Perhaps a continuous oil film on the polyethylene allowed flow—i.e., the oil was not trapped as discontinuous drops at S_{or}. Considering that F_{rro} was 24 for this experiment, the above suggestion implies that if no gel was present, the permeability to oil at a water saturation of 75.7% (from Table 2) should be 24 times less than the permeability to oil at a water saturation of 15.2%. In other words, perhaps our core was not at true irreducible oil saturation when water was injected. We will explore this possibility in future work.

Recall that the process of gel placement drove S_{or} from 25.0% to 5.6% (Table 2). However, during oil flooding after gel placement, oil returned to those locations where gelant had previously removed residual oil (see Figs. 18-20 and Figs. 23 and 26). Why did gel not permanently block these locations? Considering the size of these locations (red areas of Figs. 18-20) and the inert nature of polyethylene, it seems likely that gel formed here as effectively as in other locations. Possibly, during the oil flood after gel placement, the topography of the porous medium, combined with capillary forces, allowed the oil to rip[9,10] or dehydrate[15] gel to form pathways in the regions occupied by the original oil saturation. As mentioned earlier, this mechanism may have been operable in Berea also. However, in Berea, the gel trapped oil associated with saturations at S_{wr} before gel placement. In polyethylene, the gel trapped oil associated with saturations at S_{or} before gel placement. Perhaps the thin filaments that bridged the smaller pores in polyethylene (Fig. 4) acted as guide wires, allowing oil to breach the gel and re-occupy the observed locations.

After gel placement, the permeability to water was dramatically less than that to oil. This result suggests that the largest oil pathways shown in Figs. 18 and 20 were generally not open to water flow. Why not? One proposed possibility was that a new residual oil saturation was established in these pathways during the final water flood.[15] However, careful examination of Figs. 18-21 and Figs. 23 and 26 reveals that this did not happen. A second possibility is that elastic forces associated with the gel closed the largest oil pathways during the final water flood.[9,10] In this theory, capillary forces keep the oil pathways open during oil flooding.[9,10] (By proper labeling of our gel and fluids, we may be able to test this hypothesis in future XMT studies.) A third possibility is that the oil pathways were open during oil flooding but closed during water flooding because gels "shrink in the presence of oil but swell in the presence of water."[4-6] This proposed mechanism is troubling because in the absence of osmotic effects, the available evidence indicates that our gels do not shrink in the presence of oil and swell in the presence of water.[7,9] A fourth possiblility is that the polyethylene filaments (Fig. 4) played an important role in inhibiting water movement through these pores.

Of course, additional work will be performed to address the questions and test the hypotheses raised in this paper.

Conclusions

X-ray computed microtomography was used to investigate why gels reduce permeability to water more than that to oil in

strongly water-wet Berea sandstone and in an oil-wet porous polyethylene core. The following conclusions were reached:

1. Although the two porous media had very different porosities (22% versus 40%), the distributions of pore sizes and aspect ratios were similar.
2. A Cr(III)-acetate-HPAM gel caused comparable oil and water permeability reductions in both porous media. In both cores, the gel reduced permeability to water by a factor 80 to 90 times more than that to oil.
3. The distributions of water and oil saturations (versus pore size) were substantially different before, during, and after gel placement.
4. The disproportionate permeability reduction appeared to occur by different mechanisms in the two porous media. In Berea, gel caused disproportionate permeability reduction by trapping substantial volumes of oil that remained immobile during water flooding. With this high trapped oil saturation, water was forced to flow through narrow films, through the smallest pores, and through the gel itself. In contrast, during oil flooding, oil pathways remained relatively free from constriction by the gel.
5. In the polyethylene core, oil trapping did not contribute significantly to the disproportionate permeability reduction. Instead, oil films and a relatively small number of pore pathways provided conduits for the oil. For reasons yet to be understood, the small pore pathways appeared largely unavailable for water flow.

Nomenclature

F_{rr} = residual resistance factor
F_{rro} = residual resistance factor for oil
F_{rrw} = residual resistance factor for water
k_{ro} = relative permeability to oil
k_{rw} = relative permeability to water
R = Aspect ratio
S_{or} = residual oil saturation, %
S_w = water saturation, %
S_{wr} = residual water saturation, %

Acknowledgments

Financial support for this work is gratefully acknowledged from the National Petroleum Technology Office of the United States Department of Energy, BP-Amoco, Chevron, China National Petroleum Corp., Chinese Petroleum Corp., Marathon, Shell, and Texaco. The efforts of John Hagstrom were appreciated during the corefloods and imaging experiments. We also thank Dr. Jill S. Buckley (New Mexico PRRC) for helpful discussions and suggestions and Nelia Dunbar (New Mexico BMMR) for obtaining the electron micrographs. This research was carried out (in part) at the National Synchrotron Light Source, Brookhaven National Laboratory, which is supported by the U.S. Department of Energy, Division of Materials Sciences and Division of Chemical Sciences. The Geosciences Program of the U.S. Department of Energy (grant DE-FG02-92ER14261) funded development of the 3DMA code.

References

1. Liang, J., Sun, H., Seright, R.S.: "Reduction of Oil and Water Permeabilities Using Gels," paper SPE 24195 presented at the 1992 SPE/DOE Symposium on Enhanced Oil Recovery, Tulsa, April 22-24.
2. Seright, R.S., Liang, J., and Sun, H.: "Gel Treatments in Production Wells with Water Coning Problems," *In Situ* (1993) **17**(3) 243-272.
3. Liang, J., Lee, R.L., and Seright, R.S.: "Placement of Gels in Production Wells," *SPEPF* (Nov. 1993) 276-284; Transactions AIME 295.
4. Sparlin, D.D. and Hagen, R.W. Jr.: "Controlling Water in Producing Operation? Part 5," *World Oil* (June 1984) 137.
5. Dawe, R.A. and Zhang, Y.: "Mechanistic Study of the Selective Action of Oil and Water Penetrating into a Gel Emplaced in a Porous Medium," *J. Pet. Sci. Eng.* (1994) **12**, 113-125.
6. Mennella, A., *et al.*: "Pore-Scale Mechanism for Selective Permeability Reduction by Polymer Injection," paper SPE 39635 presented at the 1998 SPE/DOE Improved Oil Recovery Symposium, Tulsa, April 19-22.
7. Liang, J., Sun, H., and Seright, R.S.: "Why Do Gels Reduce Water Permeability More Than Oil Permeability?" *SPERE* (Nov. 1995) 282-286.
8. Zaitoun, A. and Kohler N.: "Thin Polyacrylamide Gels for Water Control in High-Permeability Production Wells" paper SPE 22785 presented at the 1991 SPE Annual Technical Conference and Exhibition, Dallas, Oct. 6-9.
9. Liang, J. and Seright, R.S.: "Further Investigations of Why Gels Reduce k_w More Than k_o," *SPEPF* (Nov. 1997) 225-230.
10. Al-Sharji, H.H., *et al.*: "Pore-Scale Study of the Flow of Oil and Water through Polymer Gels," paper SPE 56738 presented at the 1999 SPE Annual Technical Conference and Exhibition, Houston, Oct. 3-6.
11. Zaitoun, A., Bertin, H., and Lasseux, D.: "Two-Phase Flow Property Modifications by Polymer Adsorption," paper SPE 39631 presented at the 1998 SPE/DOE Improved Oil Recovery Symposium, Tulsa, April 19-22.
12. Nilsson, S., Stavland, A., and Jonsbraten, H. C.: "Mechanistic Study of Disproportionate Permeability Reduction" paper SPE 39635 presented at the 1998 SPE/DOE Improved Oil Recovery Symposium, Tulsa, April 19-22.
13. Liang, J. and Seright, R.S.: "Wall-Effect/Gel Droplet Model of Disproportionate Permeability Reduction," paper SPE 59344 presented at the 2000 SPE/DOE Improved Oil Recovery Symposium, Tulsa, April 3-5.
14. White, J.L., Goddard, J.E., and Phillips, H.M.: "Use of Polymers To Control Water Production in Oil Wells," *JPT* (Feb. 1973) 143-150.
15. Willhite, G.P., *et al.*: "Mechanisms Causing Disproportionate Permeability in Porous Media Treated With Chromium Acetate/HPAAM Gels," paper SPE 59345 presented at the 2000 SPE/DOE Improved Oil Recovery Symposium, Tulsa, April 3-5.
16. Seright, R.S.: "Improved Techniques for Fluid Diversion In Oil Recovery," final report, DOE/BC/14880-15, U.S. DOE (Jan. 1996) 97-108.
17. Dunsmuir, J.H., *et al.*: X—Ray Microtomography: A New Tool for the Characterization of Porous Media, paper SPE 22860 presented at the 1991 SPE Annual Technical Conference and Exhibition, Dallas, Oct. 6-9.
18. B.P. Flannery, *et al.*: "Three-Dimensional X—Ray Microtomography," *Science*, **237**, 1389 (1987).

19. Coles, M.E., *et al.*: "Developments in Synchrotron X—Ray Microtomography with Applications to Flow in Porous Media," *SPEREE* (Aug. 1998) 288-296.
20. Zhou, M., *et al.*: "Irreducible Water Distribution in Sandstone Rock: Two Phase Flow Simulations in CT-based Pore Network," *Phys. Chem. Earth (A)*, **25**(2), 2000, 169-174.
21. Coles, M.E., *et al.*: "Pore Level Imaging of Fluid Transport Using Synchrotron X-Ray Microtomography," paper 9628 presented at the 1996 International Symposium of the Society of Core Analysts, Montpellier, France, Sept. 8-10.
22. Hazlett, R.D., Chen, S.Y, and Soll, W.E.: "Wettability and Rate Effects on Immiscible Displacement: Lattice Boltzmann Simulation in Microtomographic Images of Reservoir Rocks," presented at the 1996 4th International Symposium on Evaluation of Reservoir Wettability and its Effect on Oil Recovery, Montpellier, France, Sept. 11-13.
23. Lindquist, W.B., *et al.*: "Pore and Throat Size Distributions Measured From Synchrotron X-Ray Tomography Images of Fountainebleau Sandstones," *J. Geophys. Research*, **105B**, (2000) 21508-21528.
24. Chatzis, I., Morrow, N.R., and Lim, H.T.: "Magnitude and Detailed Structure of Residual Oil Saturation," *SPEJ* (April 1983) 311-326.
25. Chatzis, I., Kuntamukkula, M.S., and Morrow, N.R.: "Effect of Capillary Number on the Microstructure of Residual Oil in Strongly Water-Wet Sandstones," *SPERE* (Aug. 1988) 902-912.
26. Elmkies, P. *et al.*: "Further Investigations on Two-Phase Flow Property Modification by Polymers: Wettability Effects," paper SPE 64986 presented at the 2001 SPE International Symposium on Oilfield Chemistry, Houston, Feb. 13-16.
27. Wang, D. *et al*: "Study of the Mechanism of Polymer Solution with Visco-Elastic Behavior Increasing Microscopic Oil Displacement Efficiency and the Forming of Steady Oil Thread Flow Channels," paper SPE 68723 presented at the 2001 SPE Asia Pacific Oil and Gas Conference and Exhibition, Jakarta, April 17-19.

SI Metric Conversion Factors

bbl x 1.589 873	E-01	= m^3
cp x 1.0*	E-03	= Pa?s
ft x 3.048*	E-01	= m
in. x 2.54*	E+00	= cm
mD x 9.869 233	E-04	= ?m^2
psi x 6.894 757	E+00	= kPa

*Conversion is exact.

Table 1—Proposed Mechanisms for Disproportionate Permeability Reduction

1. Gels shrink in oil but swell in water.[4-6]
2. Gravity affects gel locations in pores.[7]
3. Lubrication effects.[8]
4. During brine injection, polymer leaches from the gel and significantly decreases the brine mobility.[9]
5. Balance between capillary forces and gel elasticity affects oil and water flow differently.[9,10]
6. Gelants or gels alter rock wettability.[11,12]
7. In a given pore, gels constrict water pathways more than oil pathways. (Wall effects.)[11]
8. Pore blocking by gel droplets.[12,13]
9. Combined wall-effect and gel-droplet model.[13]
10. On a microscopic scale, water and oil follow different pathways.[7,9,12,14]
11. Gels dehydrate when oil is injected.[15]

Table 2—Fluid Saturations

	1st Berea core	2nd Berea core	Poly-ethylene core
Permeability, darcys	0.47	0.48	8.8
Porosity, %	22	22	40
First saturated with:	water	water	oil
S_w at 1st S_{wr}, %	24.7	37.3	0.0
S_w at 1st S_{or}, %	56.5	56.8	77.7
S_w at 2nd S_{wr}, %		34.3	15.2
S_w at 2nd S_{or}, %			75.0
S_w at 1st S_{or} after gel, %	47.7		94.4
S_w at S_{wr} after gel, %	29.0		75.7
S_w at 2nd S_{or} after gel, %	21.3		92.4

Table 3—Permeabilities

	1st Berea core	2nd Berea core	Poly-ethylene core
Permeability, darcys	0.47	0.48	8.8
Porosity, %	22	22	40
First saturated with:	water	water	oil
k_{ro} at 1st S_{wr}	0.82	0.79	1.0
k_{rw} at 1st S_{or}	0.16	0.18	0.50
k_{ro} at 2nd S_{wr}		0.78	0.45
k_{rw} at 2nd S_{or}			0.49
F_{rro}	15		24
F_{rrw}	1,220		2,130
F_{rrw} / F_{rro}	81		89

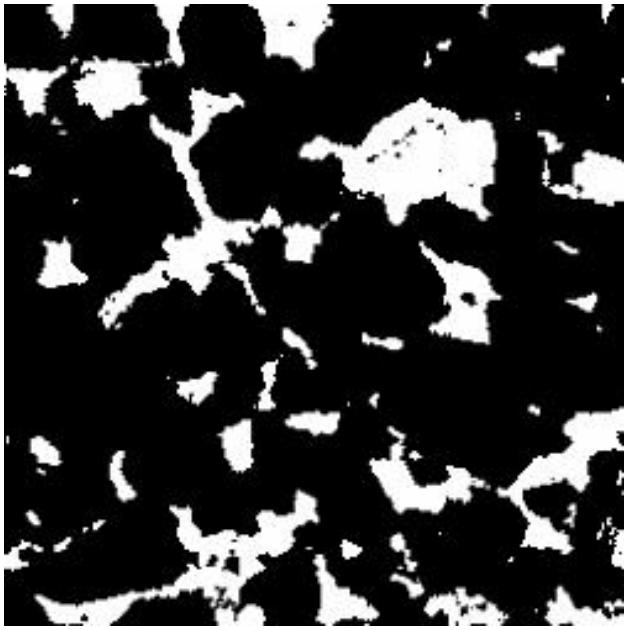

Fig. 1—XMT image cross-section of Berea. 1.15 mm x 1.15 mm.

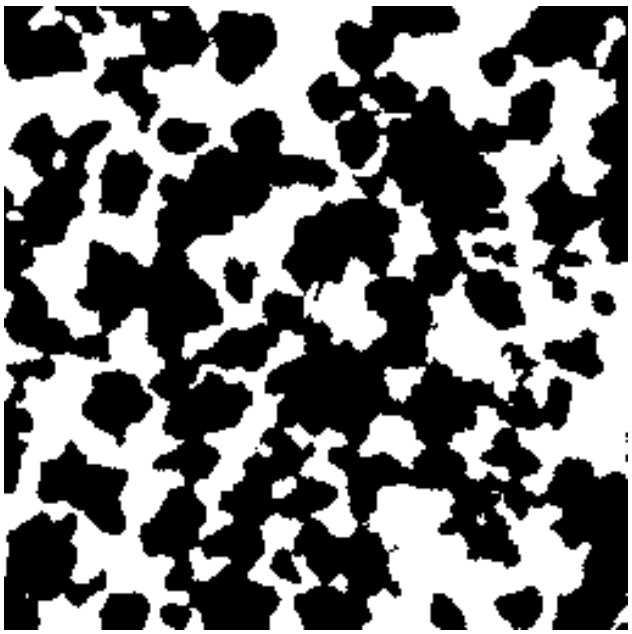

Fig. 2—XMT image cross-section of polyethylene. 1.15 mm x 1.15 mm.

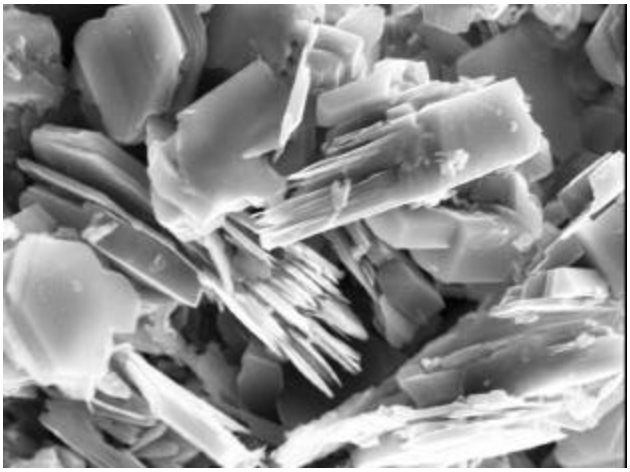

Fig. 3—Scanning electron micrograph of Berea. 30 ? m x 22 ? m.

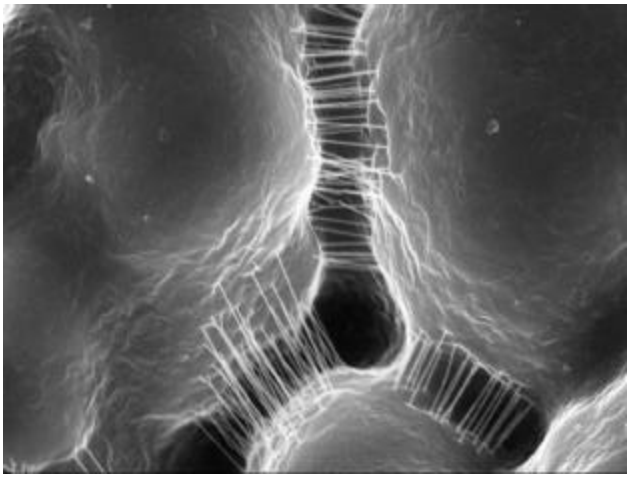

Fig. 4—Scanning electron micrograph of polyethylene. 30 ? m x 22 ? m.

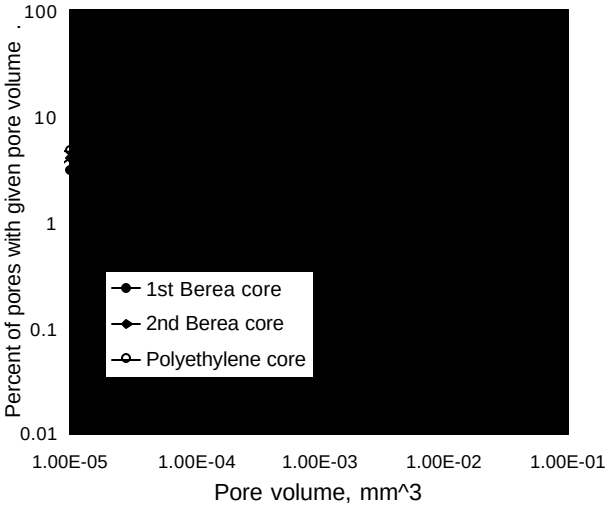

Fig. 5—Pore size distributions.

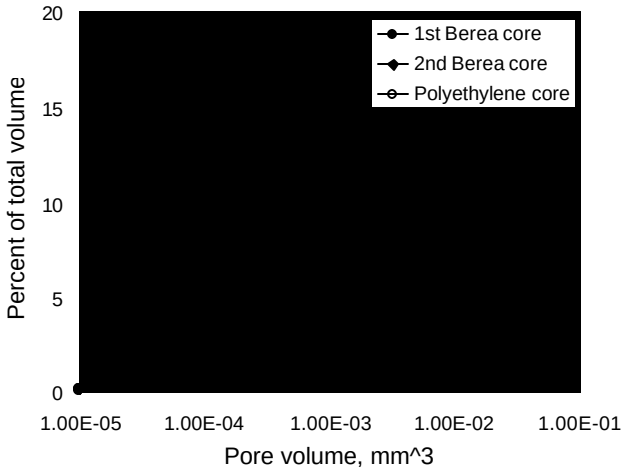

Fig. 6—Pore volume distributions.

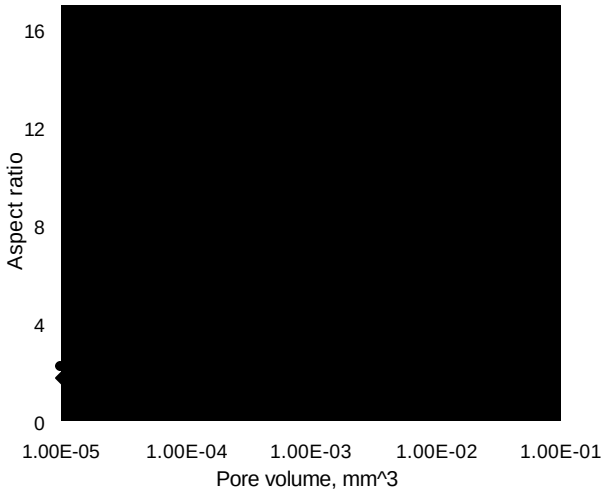

Fig. 7—Aspect ratio distributions.

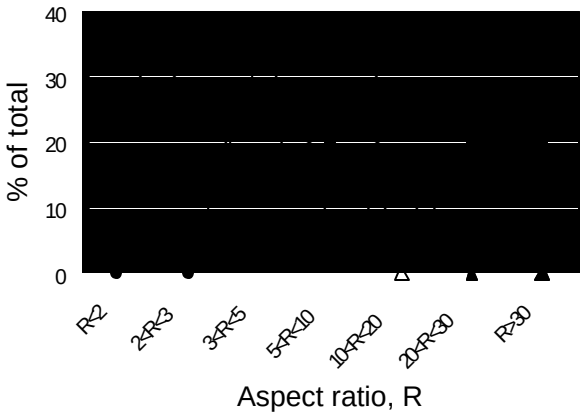

Fig. 8—Aspect ratios in Berea.

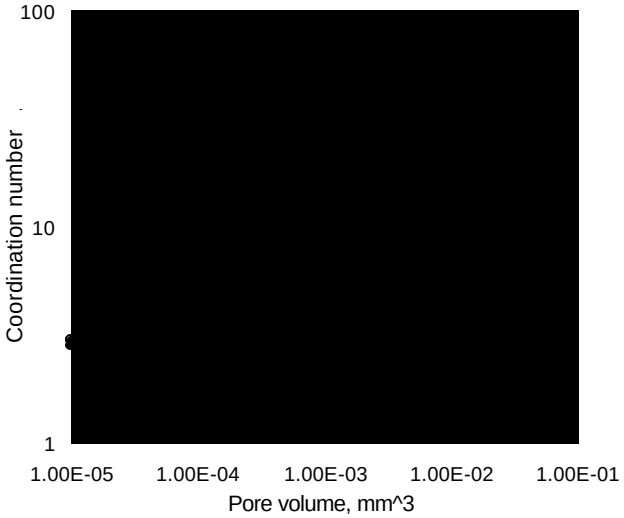

Fig. 9—Coordination number distributions.

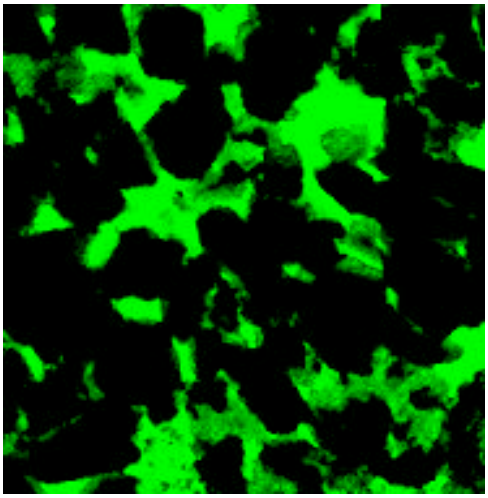

Fig. 10—Rock saturated with brine only.

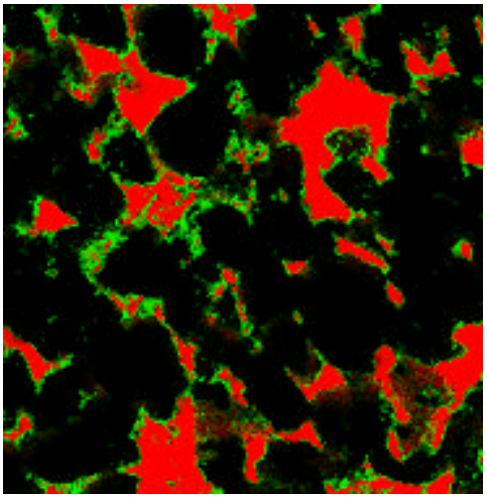

Fig. 11—At S_{wr} before gel.

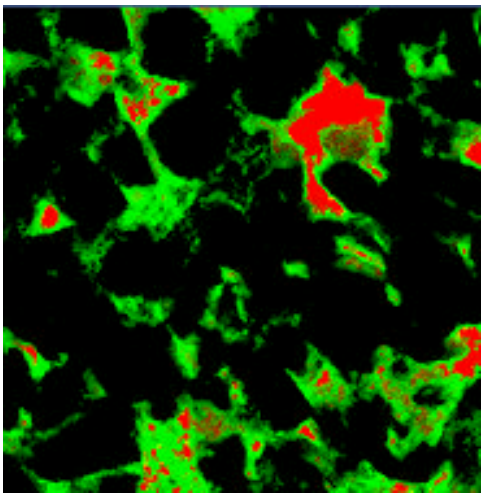

Fig. 12—At S_{or} before gel.

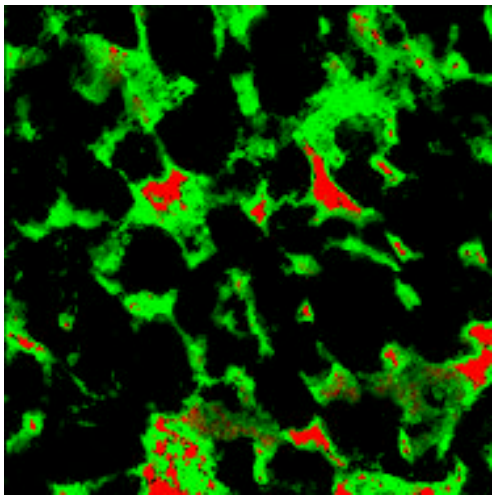

Fig. 13—After gel placement.

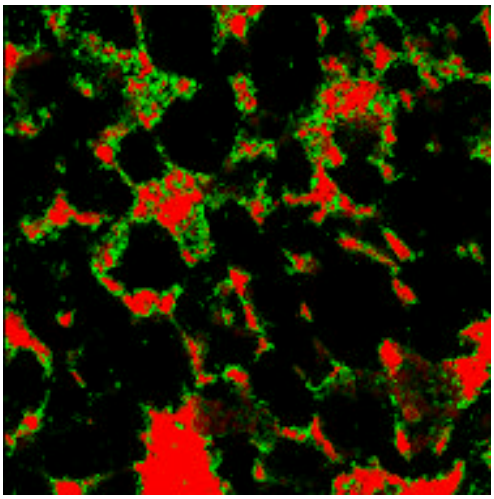

Fig. 14—At S_{wr} after gel.

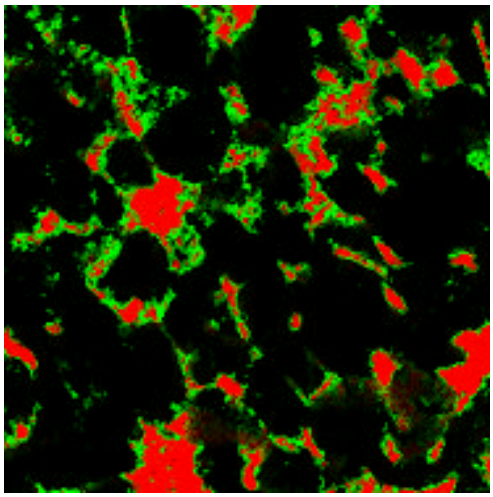

Fig. 15—At S_{or} after gel.

Berea sandstone cross-sectional image slices (1.15 mm x 1.15 mm each).
Green is water. Red is oil. Black is rock.

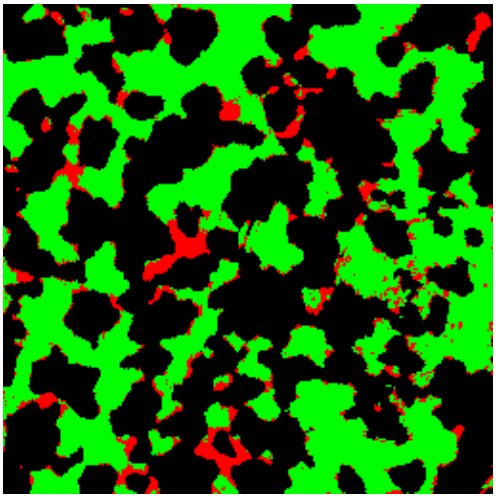

Fig. 16—At first S_{or} before gel.

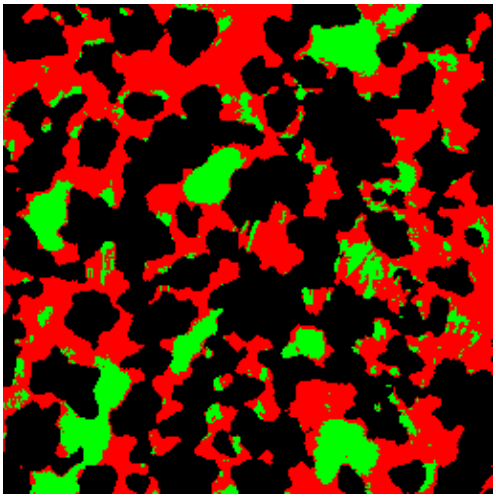

Fig. 17—At S_{wr} before gel.

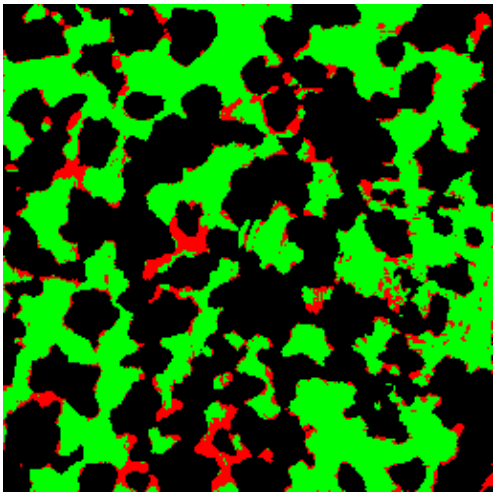

Fig. 18—At second S_{or} before gel.

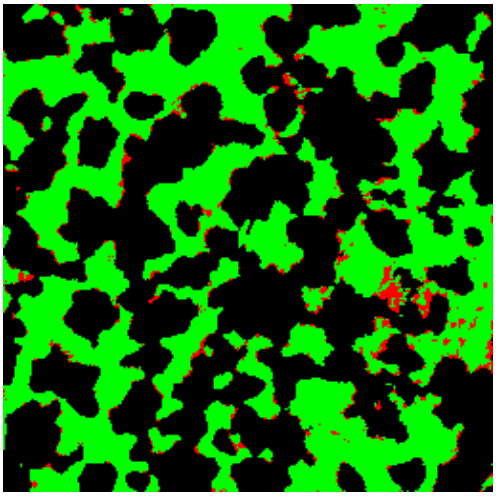

Fig. 19—After gel placement.

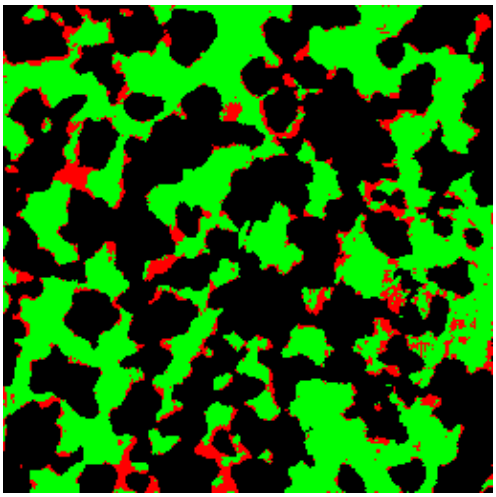

Fig. 20—At S_{wr} after gel.

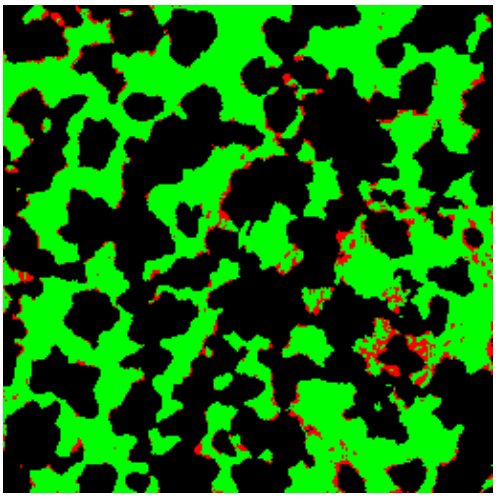

Fig. 21—At S_{or} after gel.

Polyethylene cross-sectional image slices (1.15 mm x 1.15 mm each).
Green is water. Red is oil. Black is polyethylene.

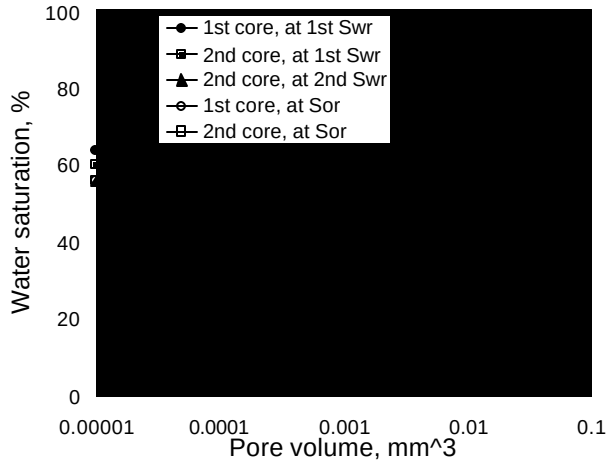

Fig. 22—Water saturations at S_{wr} and S_{or} before gel placement in Berea sandstone cores.

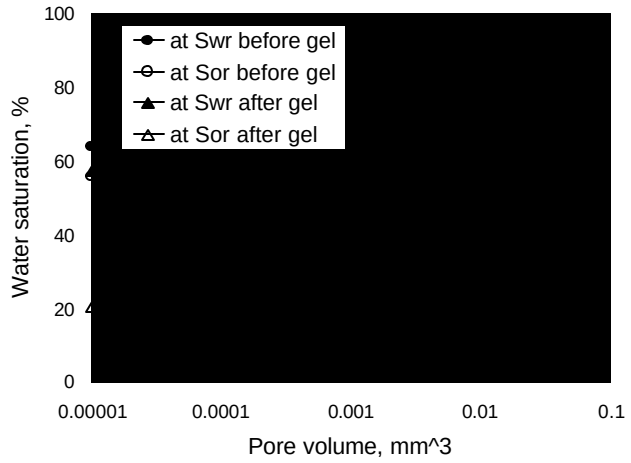

Fig. 24—Effect of gel on S_{wr} and S_{or} in Berea sandstone.

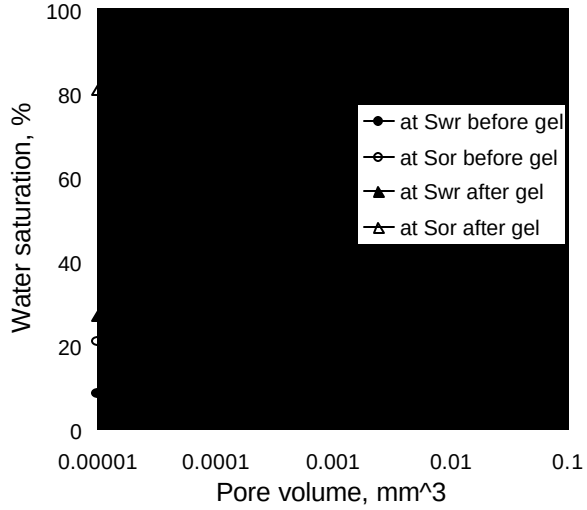

Fig. 26—Effect of gel on S_{wr} and S_{or} in polyethylene.

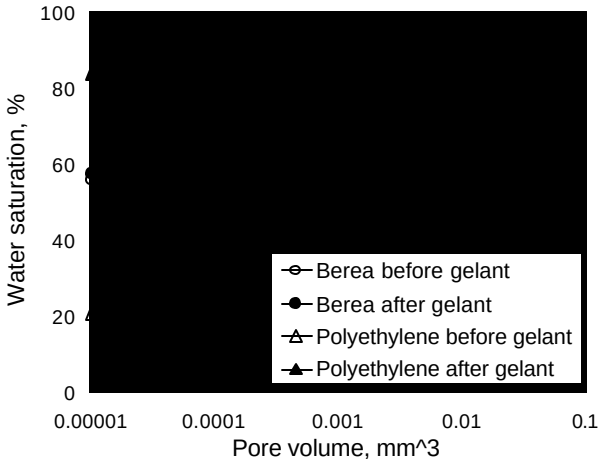

Fig. 23—Water saturations at S_{or} immediately before versus immediately after gel placement.

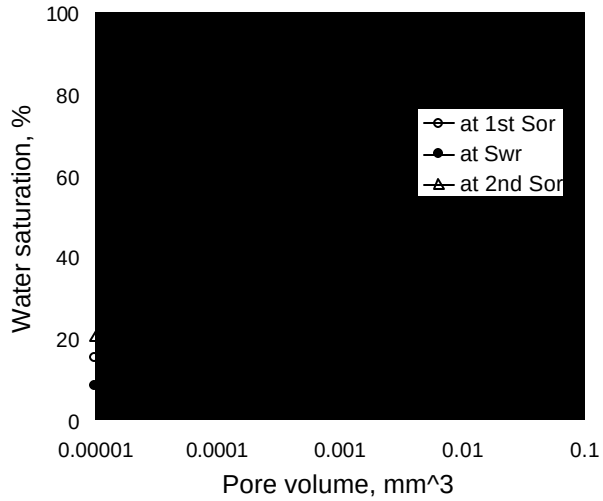

Fig. 25—Water saturations at S_{wr} and S_{or} before gel placement in the polyethylene core.